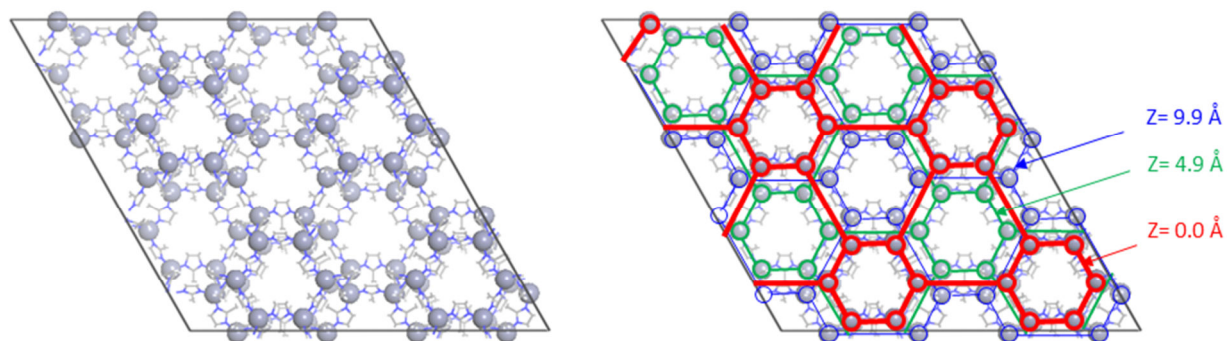


# A modelling approach for MOF-encapsulated metal catalysts and application to n-butane oxidation

*Diego A. Gomez-Gualdron,<sup>a</sup> Sean T. Dix,<sup>b</sup> Rachel B. Getman,<sup>b\*</sup> Randall Q. Snurr<sup>a\*</sup>*

<sup>a</sup> Department of Chemical and Biological Engineering, Northwestern University, 2145 Sheridan  
Road, Evanston, IL 60208, USA

<sup>b</sup> Department of Chemical and Biomolecular Engineering, Clemson University, 127 Earle Hall,  
Clemson, SC 29634-0909, USA



**Figure S1.** Left: Top view of a cut along the (111) crystallographic plane of ZIF-8. For a sufficiently large metal nanoparticle, one can imagine the plane shown could be in contact with an extended palladium flat surface (which would be in the plane of the page). Right: Same as left but with the pore structure outlined for different parallel cuts. The red color outlines the cut at  $z = 0.0 \text{ \AA}$ , which corresponds to the Pd/ZIF-8 interface. As discussed in the main text, regular hexagonal windows can provide steric constraints. Note that for  $z = 0.0 \text{ \AA}$  there are regular hexagonal openings that would be in direct contact with the palladium surface and would provide steric constraints for molecules coming towards the palladium surface (which would be in the plane of the page at  $z = 0.0 \text{ \AA}$ ) from behind the page. However, at  $z = 0.0 \text{ \AA}$  there are also irregular hexagonal openings that are too big to provide steric constraints (each irregular hexagon corresponds to a cut about half way through a sodalite cage). Interestingly, looking at the outlined cut at  $z = 4.9 \text{ \AA}$ , it is seen that half of the irregular hexagons at  $z = 0.0 \text{ \AA}$  (red) have one regular hexagonal window behind (green) only  $4.9 \text{ \AA}$  from the surface. Thus the green regular hexagons can still provide steric constraints to sufficiently long molecules coming to the Pd/ZIF-8 interface from behind the page. The remaining irregular hexagons at  $z = 0.0 \text{ \AA}$  also have one regular hexagon behind them (blue), but at  $9.9 \text{ \AA}$  from the Pd/MOF interface, and thus no steric constraints can be expected. In conclusion, according to the above model, one would expect two thirds of the catalytic surface of a palladium surface to be subject to steric constraints in a Pd/ZIF-8 material. Of course, ZIF-8 is only an example, and a major challenge is to find MOFs with appropriate pores to provide the desired steric constraints.

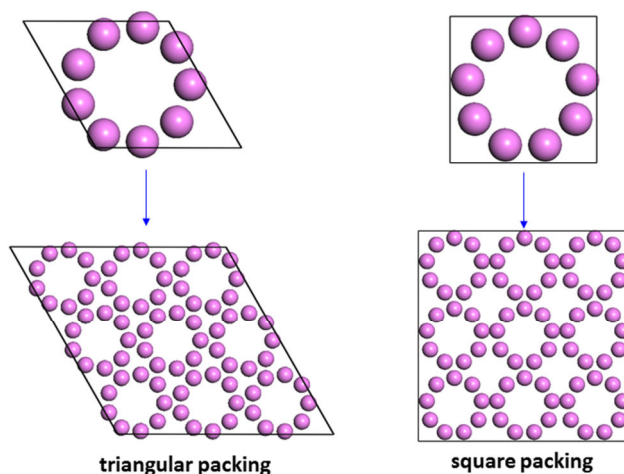


**Figure S2.** Top: Unit cells for the triangular (left) and square packing (right) of the surrogate pore. The triangular packing was used with Pd(111) surfaces, and the square packing was used with Pd(100). Bottom:  $3 \times 3$  supercell versions of the above unit cells illustrating the packing more clearly.

**Table S1.** Surrogate pore formation energies calculated as  $\Delta E_f = E_{\text{total}} - nE_{\text{atom}}$ , where  $E_{\text{total}}$  is the total energy of the pore (no Pd surface present),  $n$  is the number of atoms of the pore, and the  $E_{\text{atom}}$  is the energy for an isolated atom. Values in parenthesis correspond to the van der Waals contribution to the formation energies.

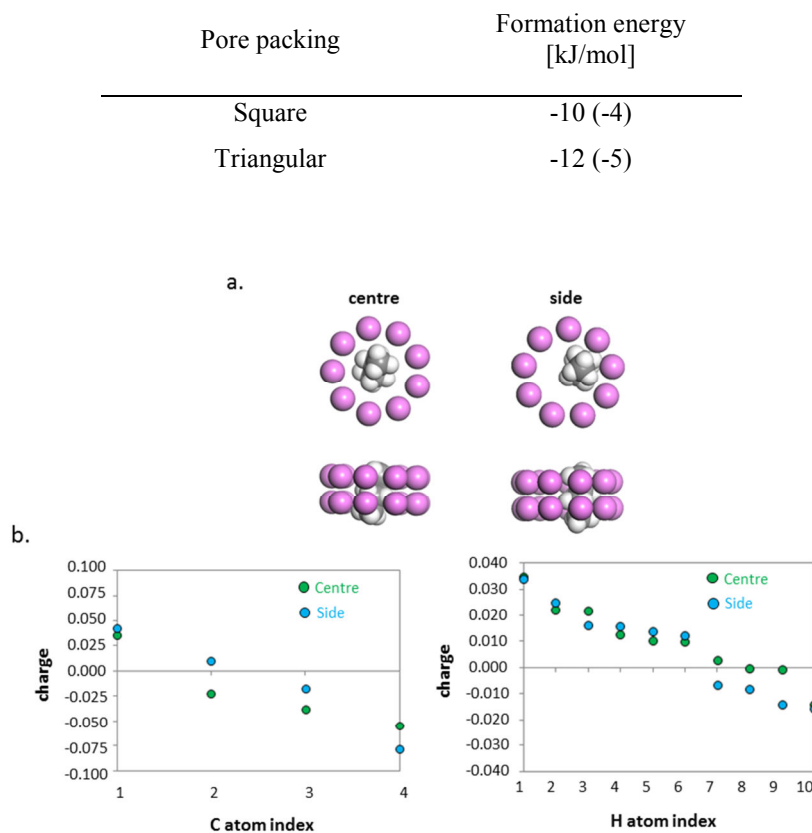


**Figure S3.** a) n-butane interacting with the surrogate pore (no Pd surface) in two possible configurations. b) Atomic charges of carbon and hydrogen atoms of n-butane for the two configurations shown in panel a).

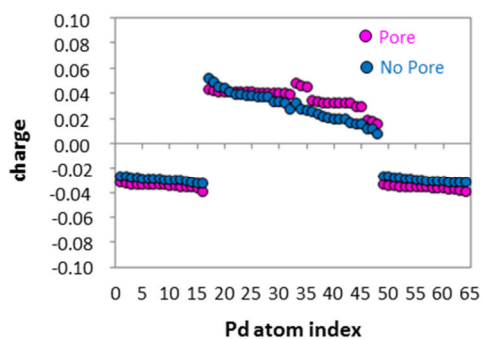


**Figure S4.** Atomic charges of the atoms of the Pd(111) slab with and without the presence of the pore. Indexes 1 to 16 and to 49 to 64 correspond to surface atoms (top and bottom layer), and all other indexes correspond to inner atoms (two intermediate layers). Note that the simulation supercell is such that there is 15 Å vacuum space between slabs in the z direction.

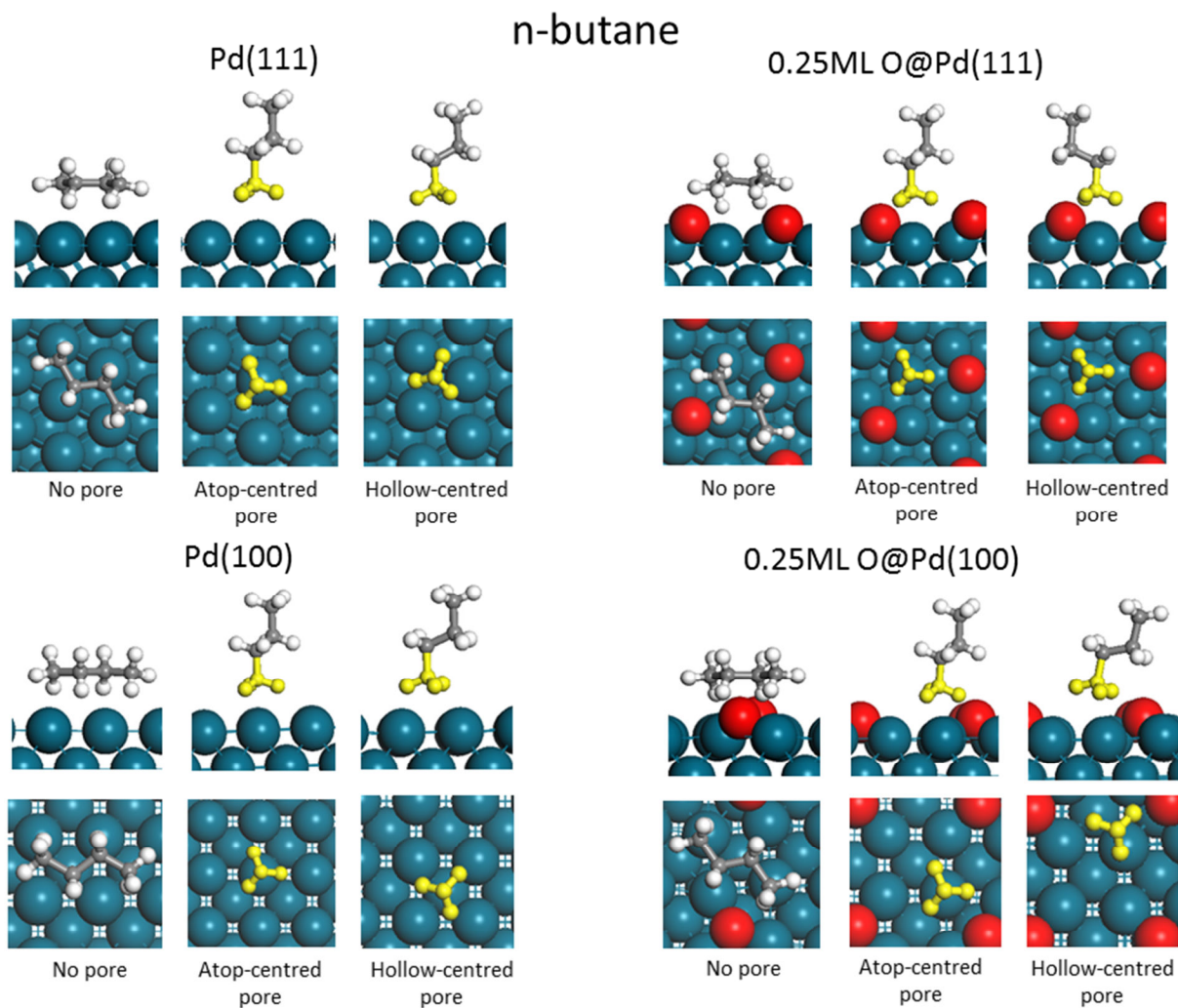


**Figure S5.** Side and top views for most stable n-butane adsorption configurations on different catalyst surfaces and conditions. For clarity, views for adsorption with the pore do not show the pore. Also, top views for adsorption with the pore only show the highlighted part of the molecule shown in the side view.

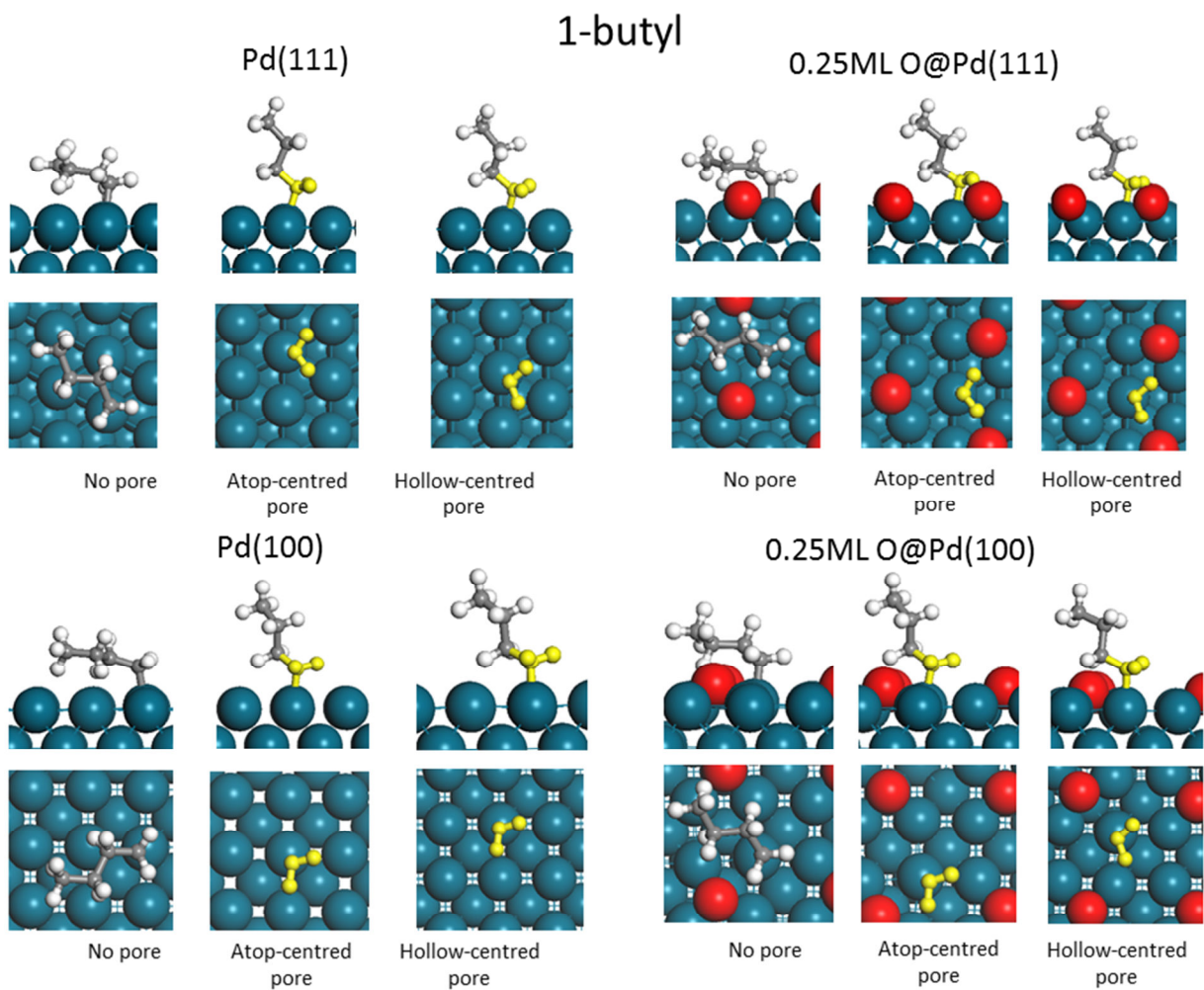


**Figure S6.** Side and top views for most stable 1-butyl adsorption configurations on different catalyst surfaces and conditions. For clarity, views for adsorption with the pore do not show the pore. Also, top views for adsorption with the pore only show the highlighted part of the molecule shown in the side view.

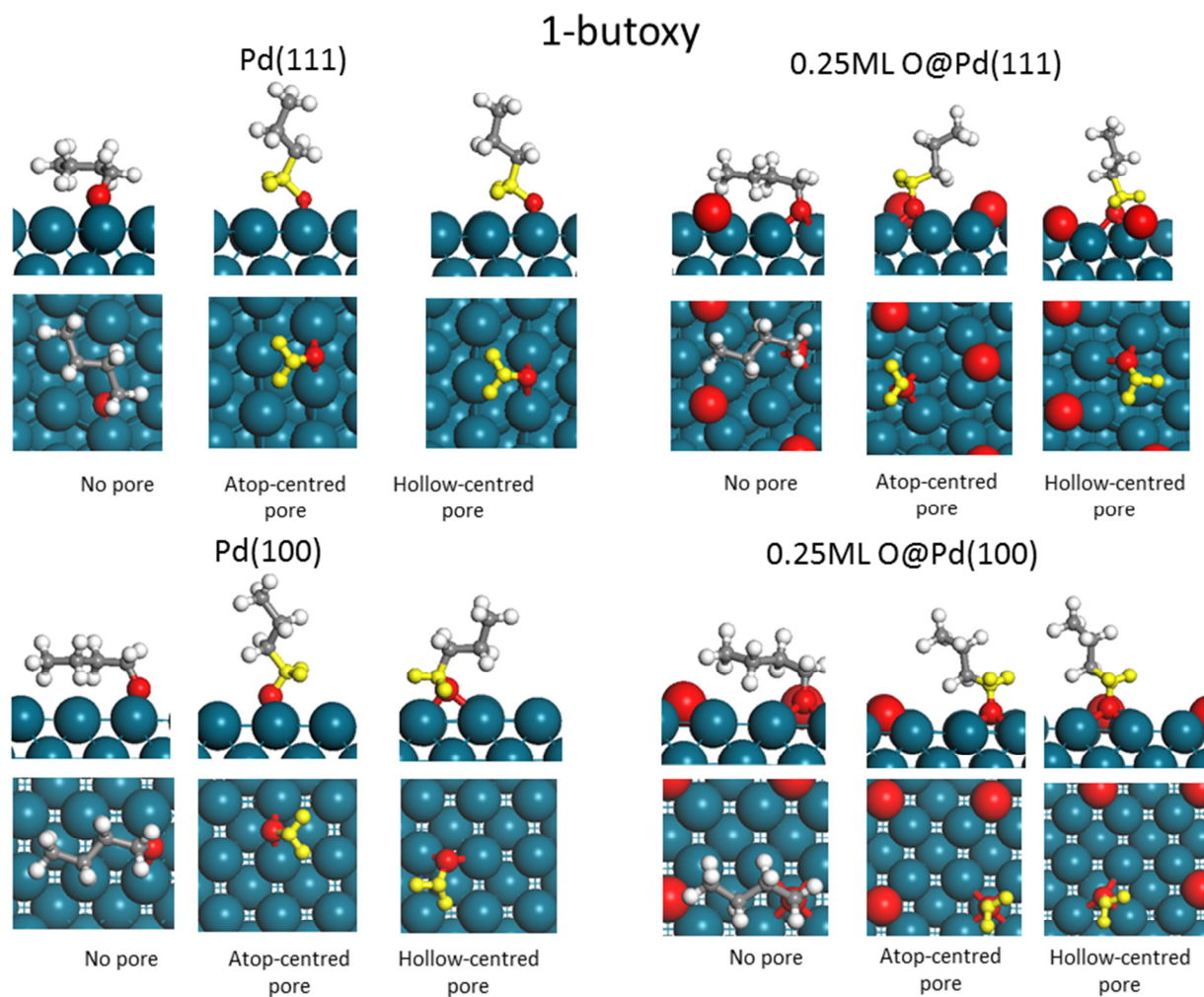


**Figure S7.** Side and top views for most stable 1-butoxy adsorption configurations on different catalyst surfaces and conditions. For clarity, views for adsorption with the pore do not show the pore. Also, top views for adsorption with the pore only show the highlighted part of the molecule shown in the side view.

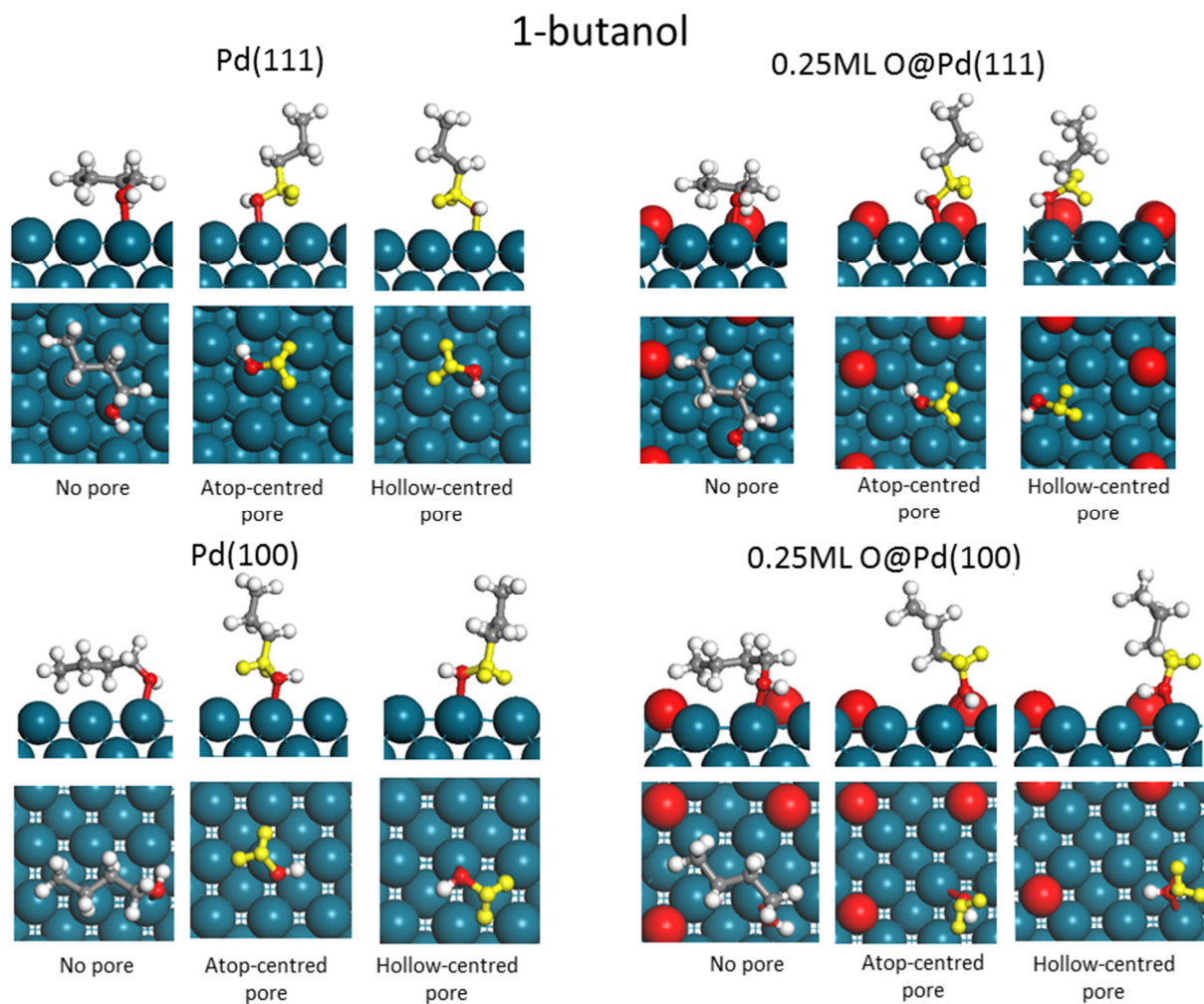


**Figure S8.** Side and top views for most stable 1-butanol adsorption configurations on different catalyst surfaces and conditions. For clarity, views for adsorption with the pore do not show the pore. Also, top views for adsorption with the pore only show the highlighted part of the molecule shown in the side view.

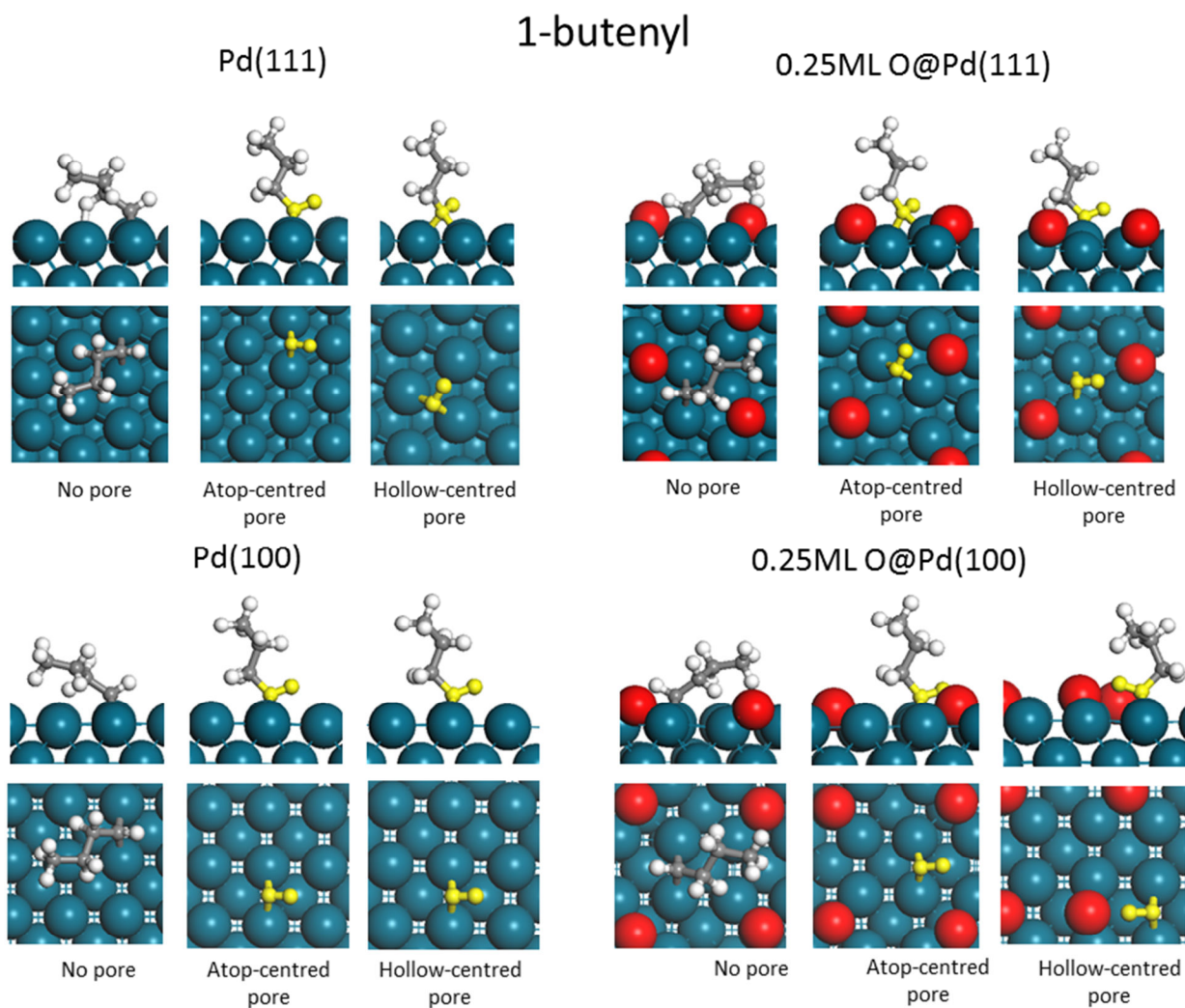


**Figure S9.** Side and top views for most stable 1-butenyl adsorption configurations on different catalyst surfaces and conditions. For clarity, views for adsorption with the pore do not show the pore. Also, top views for adsorption with the pore only show the highlighted part of the molecule shown in the side view.

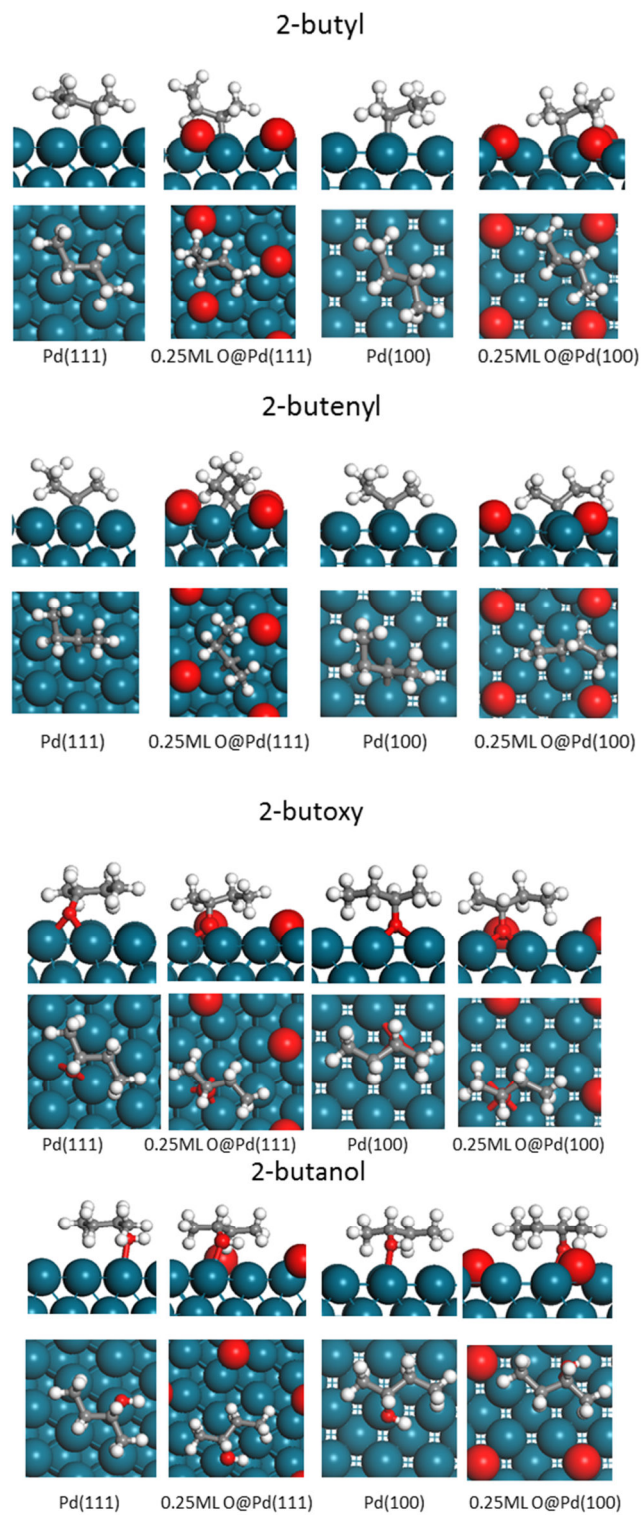


**Figure S10.** Side and top views for most stable 2-butyl, 2-butenyl, 2-butoxy, and 2-butanol adsorption configurations on different catalyst surfaces and conditions without the pore.

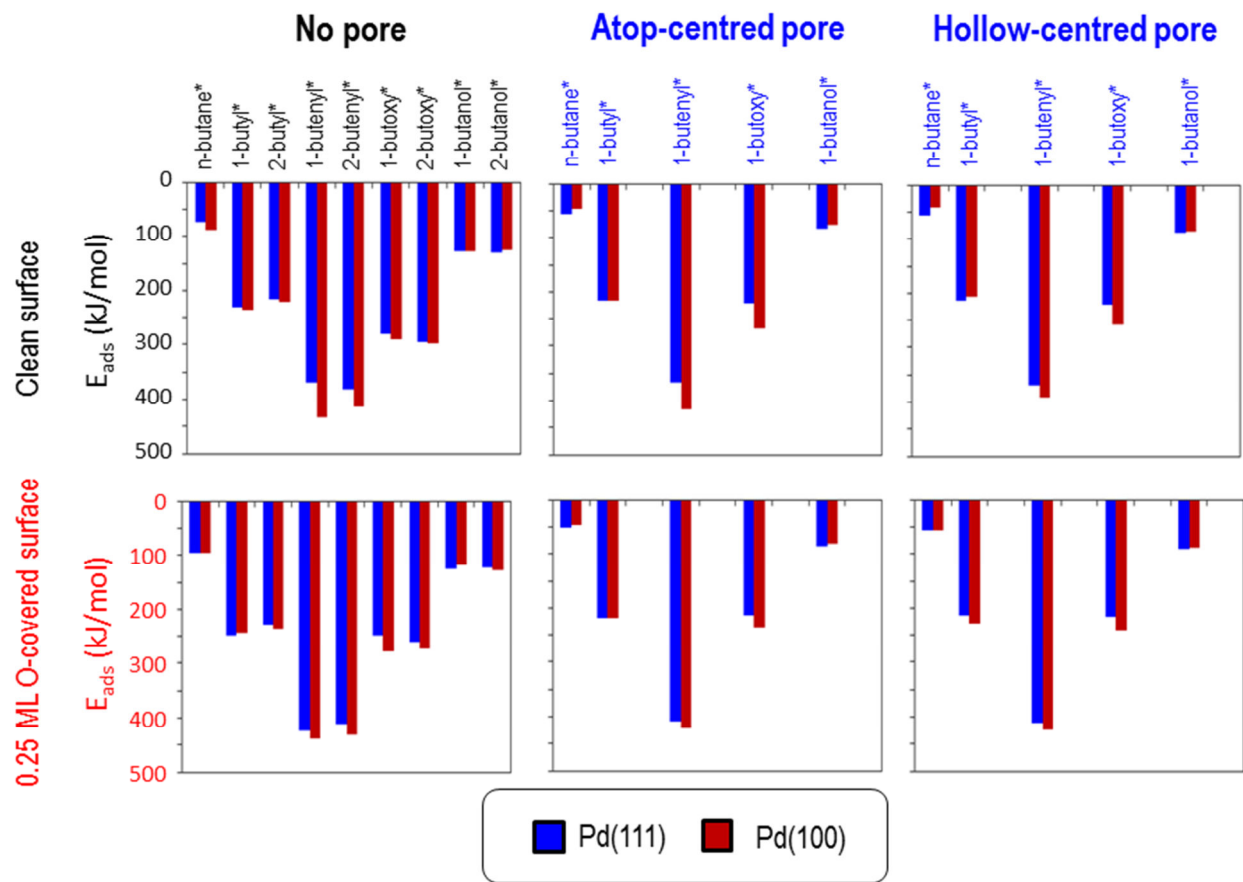


**Figure S11.** Overview of adsorption energies for all  $C_4$  species on different catalyst surfaces and conditions.

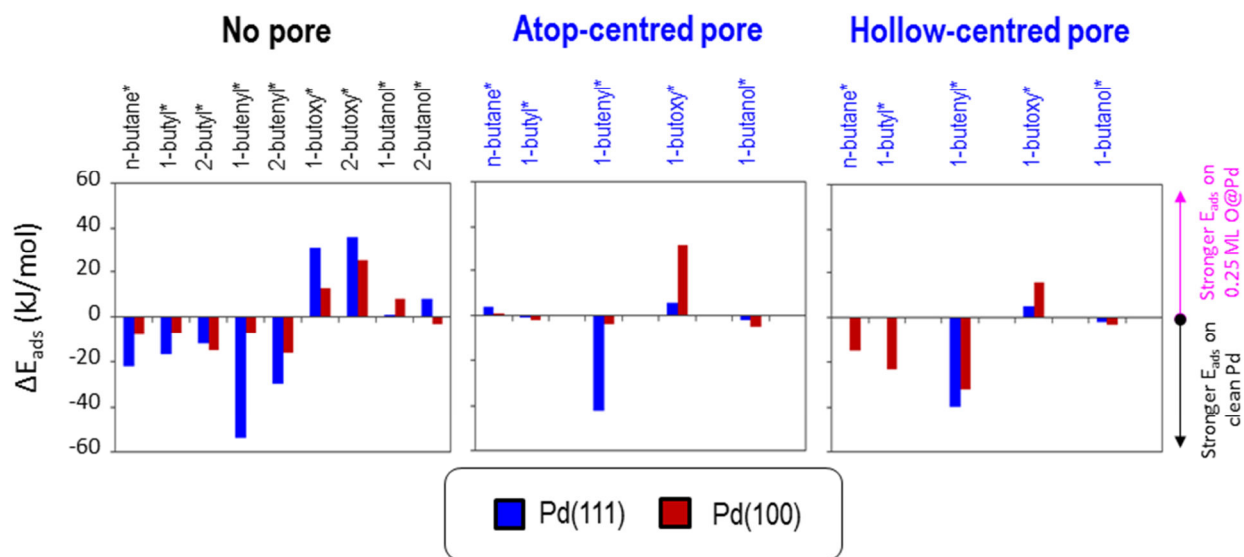


**Figure S12.** Changes in adsorption energies ( $\Delta E_{\text{ads}}$ ) of C<sub>4</sub> species when the catalyst surface changes from oxygen-covered to clean.

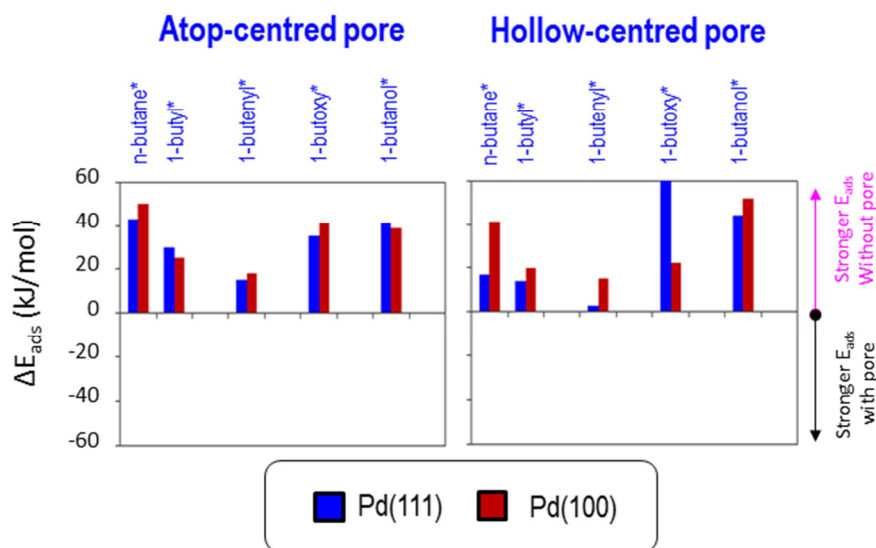


**Figure S13.** Changes in adsorption energies ( $\Delta E_{\text{ads}}$ ) of C<sub>4</sub> species when the pore is added to the catalyst surface.

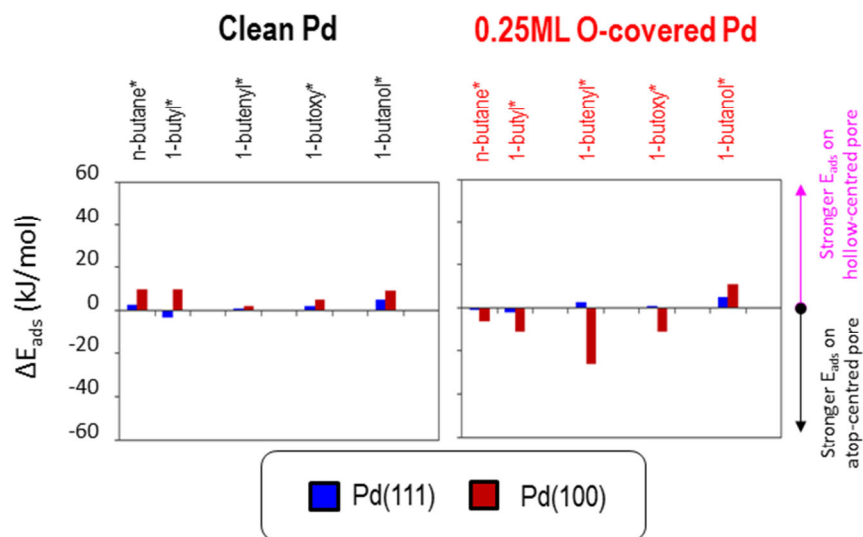


**Figure S14.** Changes in adsorption energies ( $\Delta E_{\text{ads}}$ ) when the pore position is changed from hollow-centred to atop-centred.

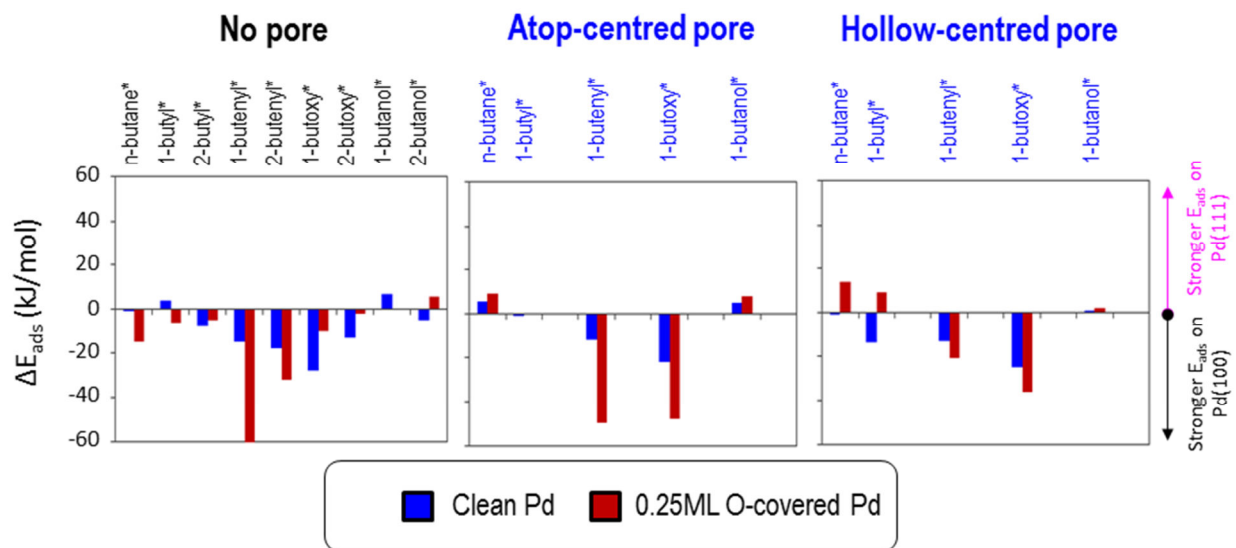


**Figure S15.** Changes in adsorption energies ( $\Delta E_{\text{ads}}$ ) when the catalyst surface changes from Pd(111) to Pd(100).

**Table S2.** Reaction energies in kJ/mol for all catalyst conditions studied in this work.

| Reaction  | Pd(111) |          | 0.25ML O@Pd(111) |          | Pd(100) |          | 0.25ML O@Pd(100) |          |
|---|---------|----------|------------------|----------|---------|----------|------------------|----------|
|   | w/ pore | w/o pore | w/pore           | w/o pore | w/pore  | w/o pore | w/pore           | w/o pore |
| $\text{O}^* + \text{H}^* \rightarrow \text{OH}^* + *$                         | -4      | -4       | -28              | -27      | -46     | -45      | -33              | -32      |
| $\text{n-butane}^* + * \rightarrow 1\text{-butyl}^* + \text{H}^*$             | -10     | 5        | 19               | 21       | -5      | 20       | -9               | 11       |
| $\text{n-butane}^* + \text{O}^* \rightarrow 1\text{-butyl}^* + \text{OH}^*$   | -14     | 1        | -8               | -6       | -50     | -25      | -42              | -20      |
| $\text{n-butane}^* + * \rightarrow 2\text{-butyl}^* + \text{H}^*$             | -       | 5        | -                | 18       | -       | 10       | -                | 10       |
| $\text{n-butane}^* + \text{O}^* \rightarrow 2\text{-butyl}^* + \text{OH}^*$   | -       | 1        | -                | -9       | -       | -35      | -                | -22      |
| $1\text{-butyl}^* + * \rightarrow 1\text{-butenyl}^* + \text{H}^*$            | -11     | 4        | 55               | 29       | -10     | -4       | -14              | -10      |
| $1\text{-butyl}^* + \text{O}^* \rightarrow 1\text{-butenyl}^* + \text{OH}^*$  | -14     | 0        | 28               | 2        | -56     | -49      | -47              | -41      |
| $2\text{-butyl}^* + * \rightarrow 2\text{-butenyl}^* + \text{H}^*$            | -       | -10      | -                | 29       | -       | -10      | -                | -15      |
| $2\text{-butyl}^* + \text{O}^* \rightarrow 2\text{-butenyl}^* + \text{OH}^*$  | -       | -14      | -                | 2        | -       | -55      | -                | -47      |
| $1\text{-butyl}^* + \text{O}^* \rightarrow 1\text{-butoxy}^* + \text{H}^*$    | 5       | -1       | 10               | -37      | -35     | -51      | -44              | -47      |
| $2\text{-butyl}^* + \text{O}^* \rightarrow 2\text{-butoxy}^* + \text{H}^*$    | -       | -25      | -                | -62      | -       | -49      | -                | -65      |
| $1\text{-butoxy}^* + \text{H}^* \rightarrow 1\text{-butanol}^* + *$           | -34     | -42      | -50              | -33      | -19     | -17      | 23               | -5       |
| $1\text{-butoxy}^* + \text{OH}^* \rightarrow 1\text{-butanol}^* + \text{O}^*$ | -32     | -38      | -23              | -6       | 26      | 28       | 56               | 27       |
| $2\text{-butoxy}^* + \text{H}^* \rightarrow 2\text{-butanol}^* + *$           | -       | -31      | -                | -25      | -       | -34      | -                | 2        |
| $2\text{-butoxy}^* + \text{OH}^* \rightarrow 2\text{-butanol}^* + \text{O}^*$ | -       | -28      | -                | 2        | -       | 12       | -                | 33       |

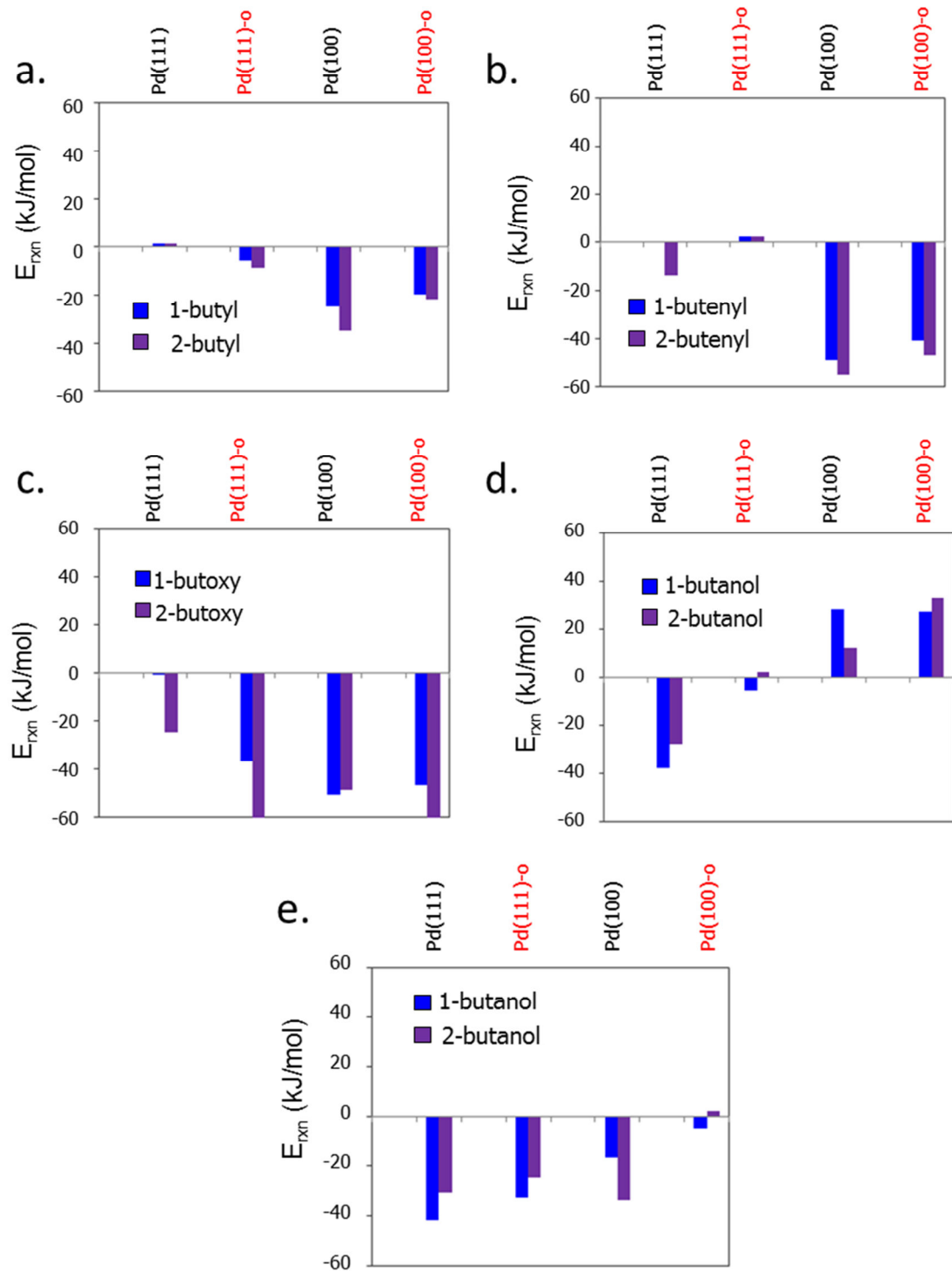


**Figure S16.** Comparison of reaction energies on the primary and secondary carbon atoms for different catalyst surfaces at different conditions in the absence of the pore. a) Reaction 8, 1-butyl vs. 2-butyl formation, b) Reaction 10, 1-butenyl vs. 2-butenyl formation, c) Reaction 11, 1-butoxy vs. 2-butoxy formation, d) Reaction 13, 1-butanol vs. 2-butanol formation (using H from hydroxyl). e) Reaction 12, 1-butanol vs. 2-butanol formation (using H bound to Pd).

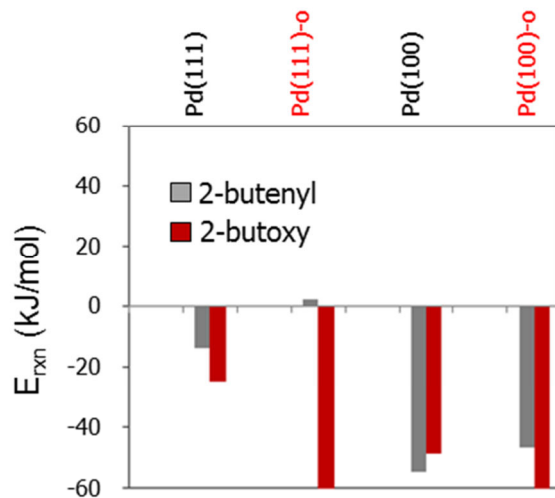


**Figure S17.** Comparison of reaction energies to form 2-butenyl (reaction 10) versus 2-butoxy (reaction 11) for different catalyst surfaces at different conditions.

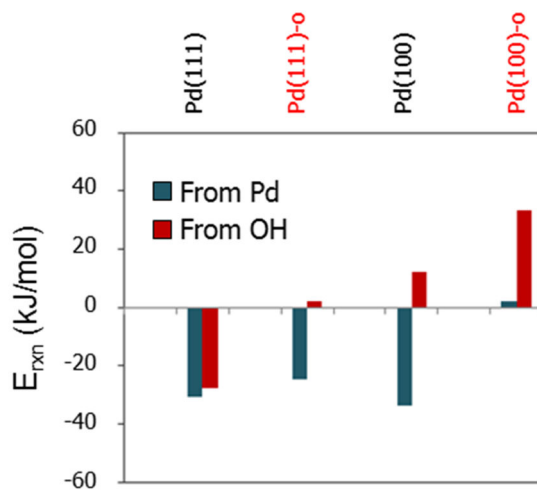


**Figure S18.** Comparison of reaction energies to convert 2-butoxy to 2-butanol using H from hydroxyl (reaction 13) versus using H bound to Pd (reaction 12).